Electronic Supplementary Information

Aliovalent metal cation doping of $La_5Ti_2AgO_7S_5$ particles for improved photocatalytic and photoelectrochemical water splitting

Yosuke Kageshima,*[ab] Shiino Otsuka,[a] Ryunosuke Iwaya,[a] Haruto Yonehara,[a] Katsuya Teshima,[ab] Kazunari Domen[bc] and Hiromasa Nishikiori*[ab]

[a.]Department of Materials Chemistry, Faculty of Engineering, Shinshu University, 4–17-1 Wakasato, Nagano 380–8553, Japan. E-mail: kage_ysk@shinshu-u.ac.jp; nishiki@shinshu-u.ac.jp

[b.]Research Initiative for Supra-Materials (RISM), Shinshu University, 4–17-1 Wakasato, Nagano 380–8553, Japan.

[c.]Office of University Professors, The University of Tokyo, 7-3-1 Hongo, Bunkyo-ku, Tokyo 113-8656, Japan.

Experimental procedures

Synthesis of LTA particles

$La_5Ti_2AgO_7S_5$ (LTA) particles were synthesized via a solid-state reaction in a sealed quartz ampule using a procedure previously described in the literature.[1] Briefly, La_2O_3 and TiO_2 were first calcined at 1273 K for 10 h or at 1073 K for 1 h, respectively, just prior to preparation of the material. To produce undoped LTA, La_2O_3, La_2S_3, TiO_2, Ag_2S and S were mixed in an Ar-filled glove box in a molar ratio of 8:12:16:4:1. During the synthesis of the doped LTA, Al_2O_3 or Ta_2O_5 were also added as dopant sources at Al/(Al+Ti) or Ta/(Ta+Ti) molar ratios in the range of 0 to 10%. Each precursor mixture was sealed in an evacuated quartz tube and subsequently heated from room temperature to 473 K over a duration of 9 min, from 473 to 673 K over 100 min and from 673 to 1273 K over 50 h, then maintained at 1273 K for 48 h.

Characterizations of materials

The morphologies and bulk compositions of the specimens were observed using field emission scanning electron microscopy (FE-SEM; Hitachi, SU8000) equipped with an energy-dispersive X-ray spectroscopy (EDS) attachment, while the crystalline structures were assessed by X-ray diffraction (XRD; Rigaku, Miniflex600) using the Cu Kα line. The optical properties of the materials were evaluated using ultraviolet-visible-near-infrared diffuse reflectance (DR) spectroscopy (Jasco, V-770), employing an integrating sphere. The surface elemental compositions of the particulate specimens were analysed by X-ray photoelectron spectroscopy (XPS; Ulvac-Phi, PHI Quantera II) employing the Al Kα line.

Photocatalytic reactions

Prior to the photocatalysis experiments, hydrogen-evolving Pt or oxygen-evolving IrO_x cocatalysts were loaded on the LTA particles.[1] Pt-modified LTA was obtained by impregnation with H_2PtCl_6 and subsequent heat treatment at 473 K for 2 h under a continuous flow of 3.95% H_2 diluted with N_2. IrO_x-modified specimens were prepared by impregnation with Na_2IrCl_6 followed by heating at 623 K for 1 h in air.

Photocatalysis trials were performed in a Pyrex top-irradiation reaction vessel connected to a glass closed gas circulation system. An aqueous solution containing 10 mM Na_2S and 10 mM Na_2SO_3 as sacrificial electron donors was employed during the hydrogen evolution half-reaction whereas 10 mM $AgNO_3$ was used as the sacrificial electron acceptor and 0.1 g La_2O_3 was used as a pH adjuster for the oxygen evolution half-reaction. In each experiment, a 0.2 g quantity of photocatalytic particles was suspended in 100 mL of the reaction solution after which air was removed and Ar was introduced to a pressure of approximately 10 kPa. A 300 W Xe lamp

equipped with a cold mirror and a long-pass filter (λ = 420 to 800 nm) was employed as the light source. The amounts of evolved gases were quantified using a gas chromatograph (Shimadzu, GC-8A) connected to the reaction system, employing Ar as the carrier gas.

(Photo)electrochemical measurements

Photoanodes were prepared by the particle transfer (PT) method.[2] During this process, the photocatalytic particles were applied to a primary glass substrate by drop-casting a suspension of the particles in isopropanol, followed by drying in air. Subsequently, a Ti backside electrode was deposited on the particles using radio frequency magnetron sputtering without heating the LTA-coated substrate. The composite formed by combining the LTA particles with the Ti layer served as a photoanode after being fixed on a secondary glass substrate using double-sided carbon tape and the removal of excessive particles by sonication.

A typical three-electrode configuration was used to assess the photoelectrochemical (PEC) performance of each photoanode. In these trials, a Ag/AgCl electrode in a saturated aqueous KCl solution and a Pt coil served as the reference and counter electrodes, respectively. A cobalt-phosphate (CoPi) cocatalyst was electrodeposited on the photoanodes in an aqueous solution containing 0.5 mM $Co(NO_3)_2$ and 0.1 M potassium phosphate buffer (KPi; 0.05 M KH_2PO_4/0.05 M K_2HPO_4). A constant potential of 1.1 V vs. Ag/AgCl was applied to the electrode for 100 s during electrodeposition of the CoPi.[3] During assessments of PEC methanol oxidation using bare LTA or of oxygen evolution by CoPi-modified specimens, a stirred aqueous electrolyte containing 0.5 M Na_2SO_4 (having an unadjusted pH of approximately 6) was employed, with or without methanol, respectively. Simulated sunlight adjusted to be equivalent to AM 1.5G radiation was used. A 300 W Xe lamp equipped with a monochromator was used as the light source in incident-photon-to-current conversion efficiency (IPCE) trials and the photon flux of the monochromatic light was determined with a calibrated Si photodiode.

During each impedance measurement, an LTA particles/Ti foil assembly fabricated through the PT method was fixed onto a secondary glass substrate using an epoxy resin instead of the double-sided carbon tape. Mott–Schottky plots of these LTA-based photoanodes under dark conditions were obtained by applying a 5 kHz potential frequency and a 10 mV AC voltage. A stirred 1 M KPi aqueous electrolyte (adjusted to pH = 7) purged with Ar was employed in these experiments.

Results and discussion

Optimisations of cocatalyst loading amounts

The cocatalyst loadings for the photocatalytic hydrogen or oxygen evolution half-reactions were optimised, with the results presented in Fig. S1. The bare LTA photocatalysts were capable of generating small amounts of hydrogen or oxygen but increased cocatalyst amounts provided higher photocatalysis rates. In contrast, excess loadings decreased the photocatalytic activity, possibly because of the trade-off relationship between the acceleration of surface reaction kinetics and light shielding by the surface modifier.[4] A 0.5 wt% Pt loading was determined to be optimal with regard to the photocatalytic hydrogen evolution half-reaction whereas an IrO_x loading equivalent to 2.0 wt% Ir metal was suitable for the oxygen evolution half-reaction.

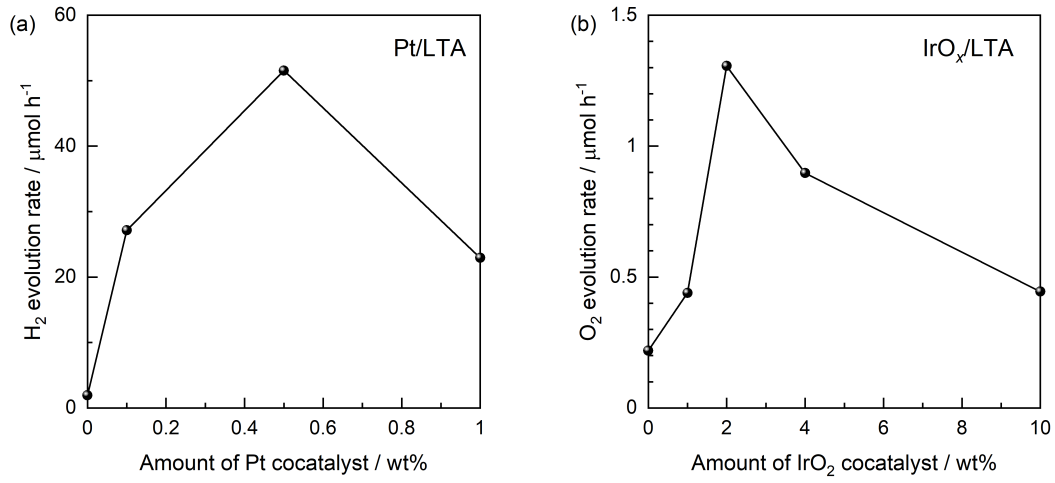

Fig. S1 Photocatalysis rates (a) during the hydrogen evolution half-reaction using Pt-modified LTA as a function of the Pt cocatalyst loading and (b) during the oxygen evolution half-reaction using IrO_x-modified LTA as a function of the IrO_x cocatalyst loading (as Ir metal).

Characterizations of doped LTA particles

SEM images of the LTA particles are presented in Fig. S2 and show that each specimen comprised rod-like crystals approximately 1 μm in diameter and 10 μm in length. Doping with Al^{3+} or Ta^{5+} had a minimal effect on the morphology of these particles regardless of the doping level.

DR spectra of the LTA particles are presented in Fig. S3. The Al:LTA specimens exhibited absorption edges almost identical to that of the original LTA regardless of the doping level (Fig. S3a). However, the absorption edges for the Ta:LTA samples were slightly red-shifted with increasing of degree of doping (Fig. S3b). In addition, increasing the extent of Ta doping provided greater absorbance at wavelengths longer than the absorption edge, implying the presence of defect sites.[5]

XRD patterns for the synthesized materials are shown in Fig. S4. These patterns confirm that the types or amount of dopant barely affected the crystalline structure of the LTA particles.

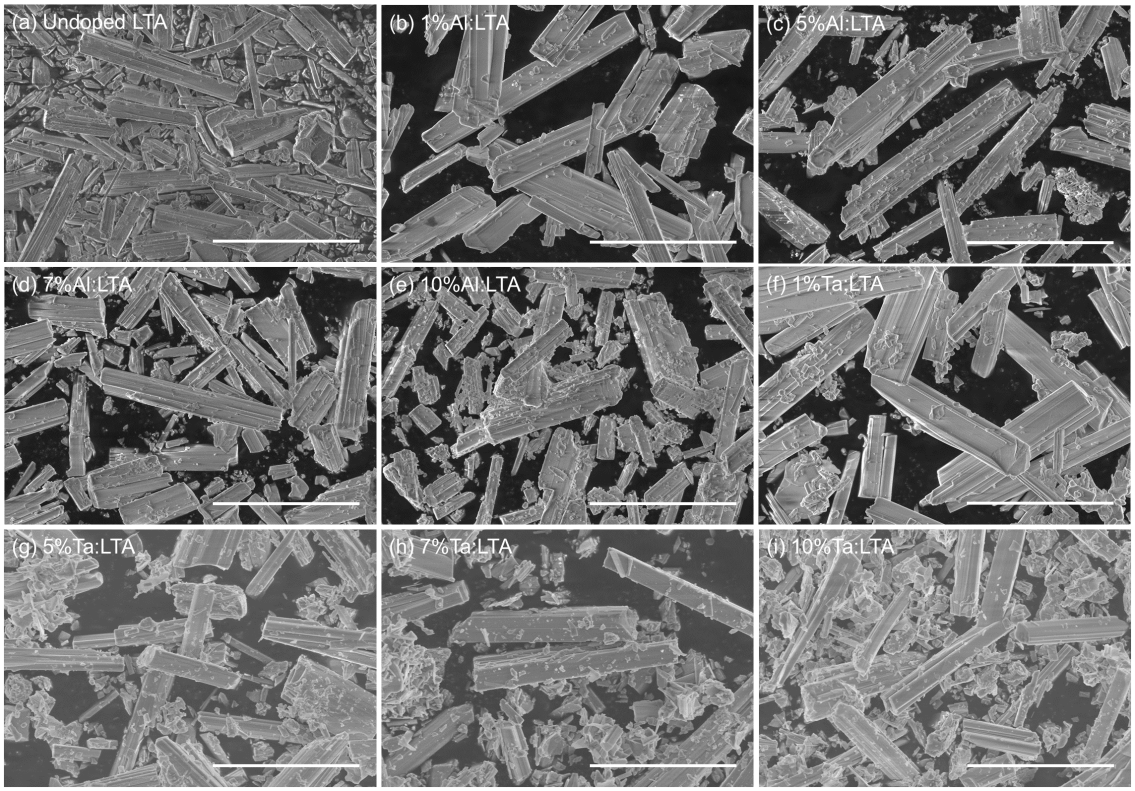

Fig. S2 SEM images of (a) undoped LTA particles, (b - e) Al:LTA with different Al doping levels, and (f - i) Ta:LTA with different Ta doping levels. Scale bars: 10 μm.

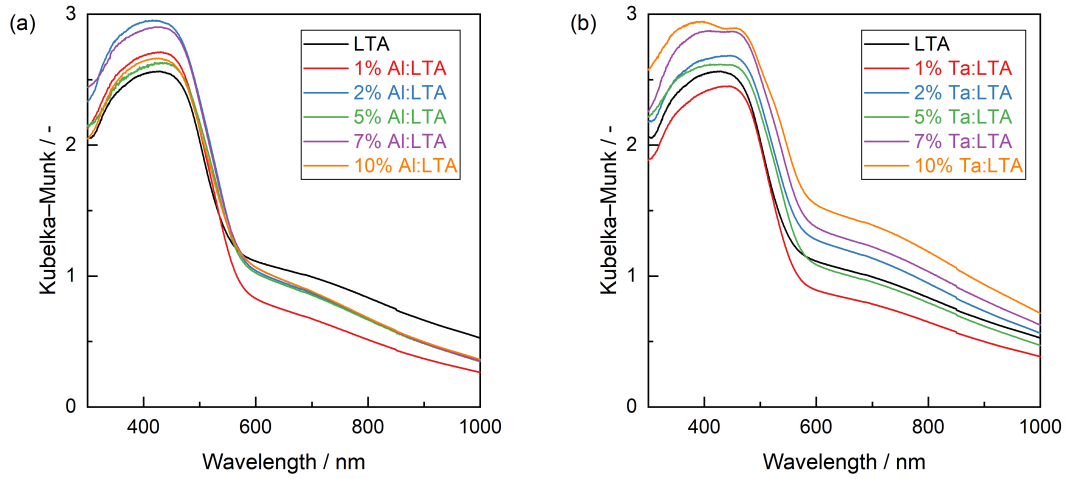

Fig. S3 DR spectra of (a) Al:LTA and (b) Ta:LTA particles with different doping levels.

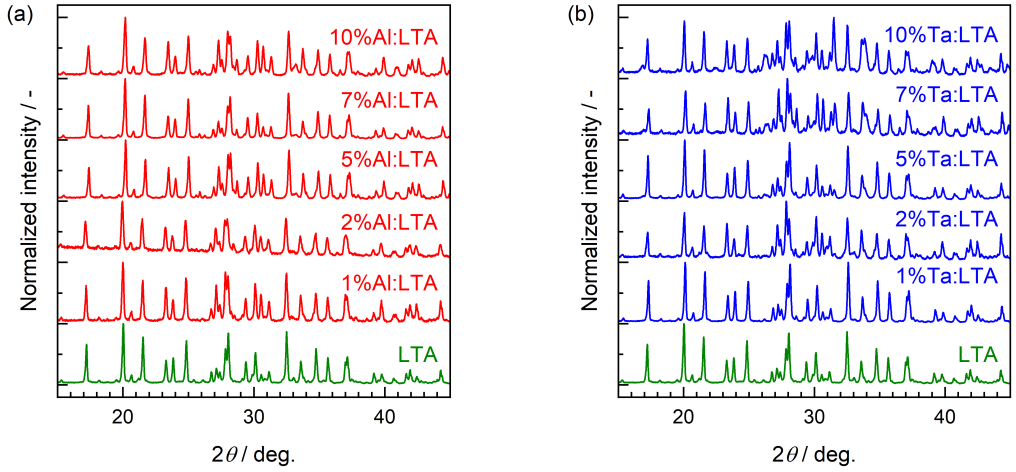

Fig. S4 XRD patterns for (a) Al:LTA and (b) Ta:LTA particles with different doping levels.

Distribution and homogeneity of the dopant species

We evaluated the actual doped amounts and doping homogeneity through EDS and XPS measurements. The bulk atomic compositions of Ta:LTA specimens determined by EDS were presented in Fig. S5. It should be noted that the quantification of small amounts of Al dopant was difficult at the present stage because of the interference by the Al filler contained in the double-sided carbon tape for SEM observation, and thus that only the EDS results obtained from Ta:LTA were presented here. The amount of dopant actually incorporated in the bulk of LTA crystalline lattice monotonically increased according to the increasing of the amount of dopant precursor. The measured values appeared almost consistent to the precursor amount at doping levels up to approximately 5 mol%, while further increasing of dopant precursor tended to cause the smaller actual doped amount compared to the expected values. This tendency well agreed with the XRD results presented in the main manuscript, in which the diffraction peak shifts plateaued at doping levels around 10 mol%. Meanwhile, the XPS signals observed from Al:LTA and Ta:LTA with a 5 mol% doping level were summarized in Fig. S6. Dopant concentrations at the surface were almost independent of the type of dopant, giving an Al/(Al+Ti) molar ratio of 0.10 and a Ta/(Ta+Ti) molar ratio of 0.079. It should be noted that the surface dopant concentrations were slightly larger than the precursor amount. Considering both EDS and XPS results, it can be concluded that almost all dopant precursor was doped into the lattice at doping levels up to 5 mol% but a part of precursor remained undoped at larger doping levels, and that there was a gradient in dopant concentration from surface toward inside of an LTA crystalline particle rather than the uniform doping throughout the crystal.

Spatial distribution and homogeneity of dopant were further assessed from the EDS mapping images (Fig. S7). Signals derived from the dopants (Al or Ta) distributed in a relatively uniform manner throughout the whole photocatalytic crystalline particles. Additionally, local bright spots that indicate the inhomogeneous distribution of the elements and/or segregation of some impurities were not observed. Thus, it can be considered that the present dopant species might be uniformly doped into the crystalline particles. The excess dopants that were not doped into the photocatalyst crystals for the case of relatively high doping levels around 10 mol% may exist as individual nanoparticles separately from the LTA particles, rather than as some fragment-like impurity nanoparticles attached to the LTA surface.

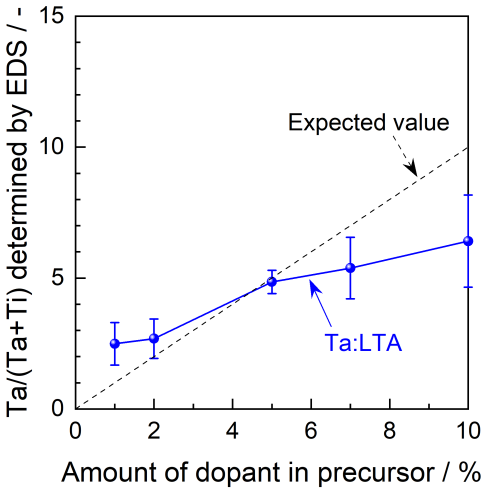

Fig. S5 Elemental Ta/(Ta+Ti) ratios in the bulk LTA particles determined by EDS.

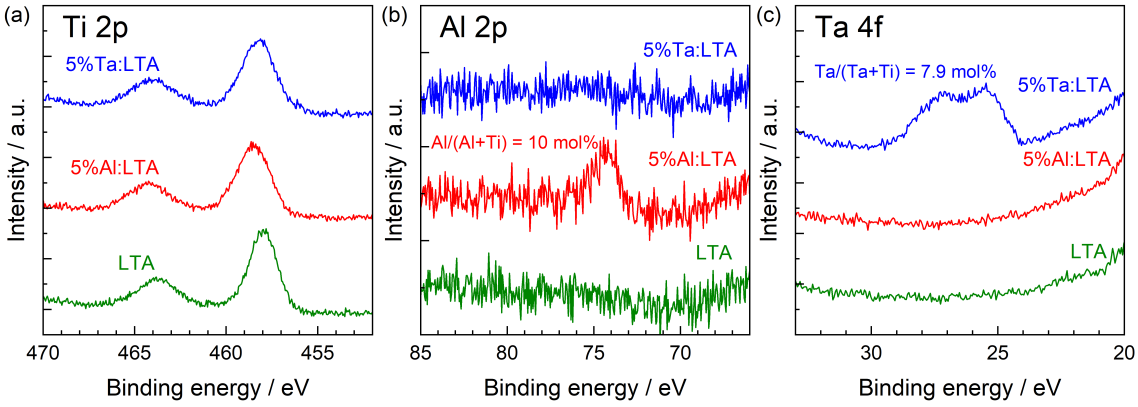

Fig. S6 (a) Ti 2p, (b) Al 2p, and (c) Ta 4f XPS signals obtained from the LTA and doped LTA specimens.

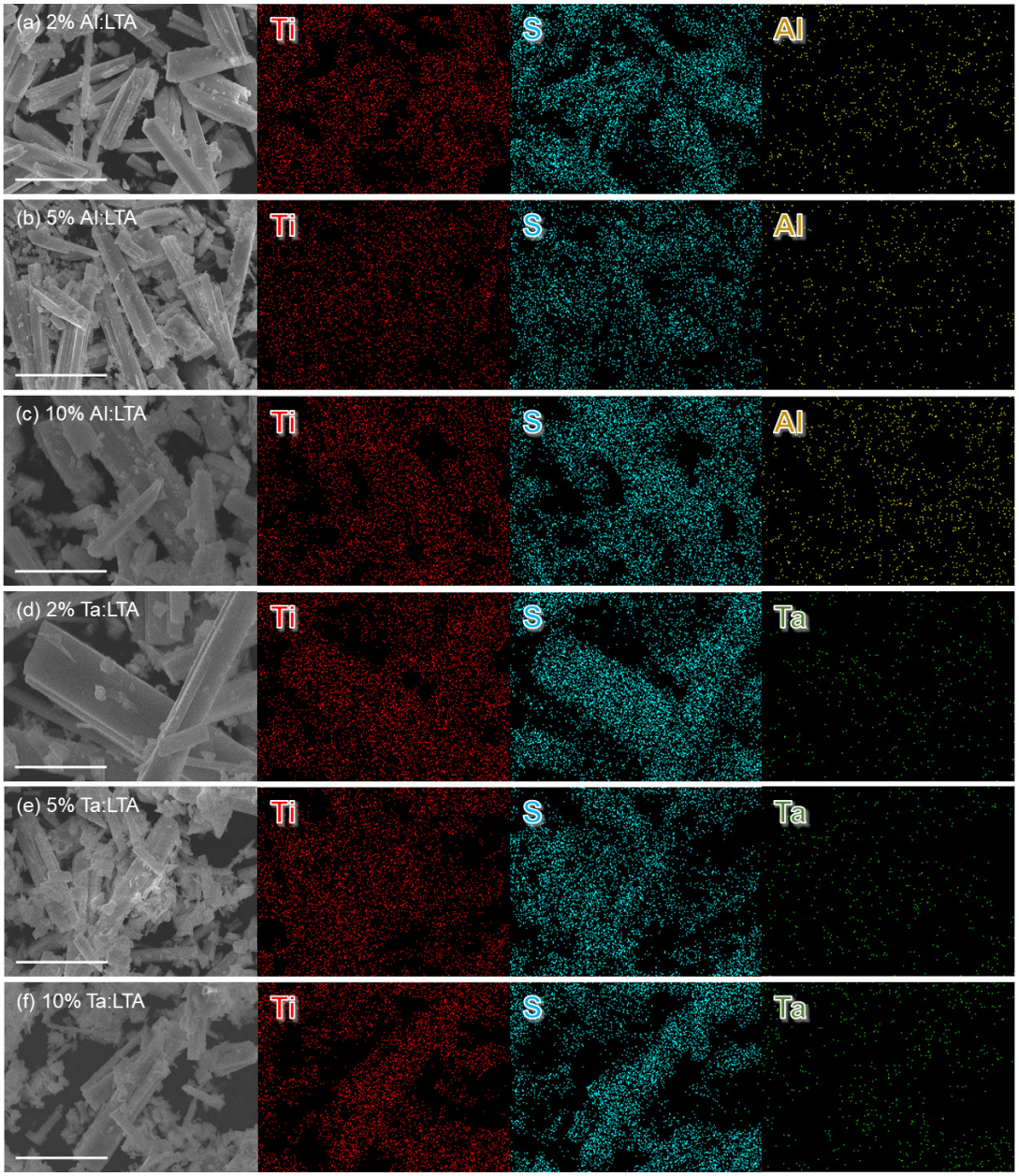

Fig. S7 SEM and EDS mapping images obtained from LTA particles doped with (a) 2%, (b) 5%, and (c) 10% Al, or (d) 2%, (e) 5%, and (f) 10% Ta. Scale bars: 10 μm.

Effects of doping levels on photocatalytic and PEC activities

The time courses of the photocatalytic hydrogen or oxygen evolution half-reactions are summarized in Fig. S8. All specimens were found to be capable of promoting steady hydrogen or oxygen evolution under visible light. The initial photocatalysis rates based on these data are presented in Fig. 2 in the main manuscript.

The doping levels for photoanode applications were separately optimised based on the PEC performance during methanol oxidation, with the results presented in Fig. S9a. The anodic photocurrent was found to gradually increase with increasing extent of Ta doping, although an excess of this dopant reduced the photocurrent. On the basis of these trials, 5 mol% Ta doping was evidently optimal. The photocurrents generated using the Al:LTA specimens were lower than those provided by the undoped material irrespective of the doping level. On this basis, the PEC oxygen evolution results obtained using CoPi-modified LTA, 5%Al-doped LTA and 5%Ta-doped LTA photoanodes are compiled in Fig. 3 in the main manuscript.

Typical current-potential curves acquired during methanol oxidation using undoped LTA, Al:LTA and Ta:LTA photoanodes are provided in Fig. S9b. The 5%Ta-doped LTA generated a higher anodic photocurrent than the undoped LTA over essentially the entire potential region while the 5%Al-doped specimen showed greatly decreased performance, especially at a negative applied potential. These results are generally consistent with the trends observed during the PEC oxygen evolution experiments as discussed in the main manuscript.

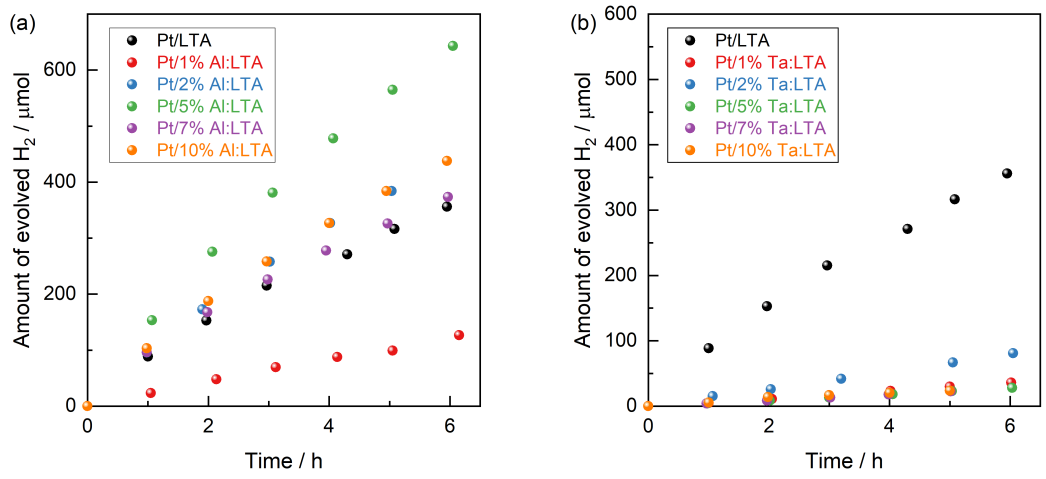

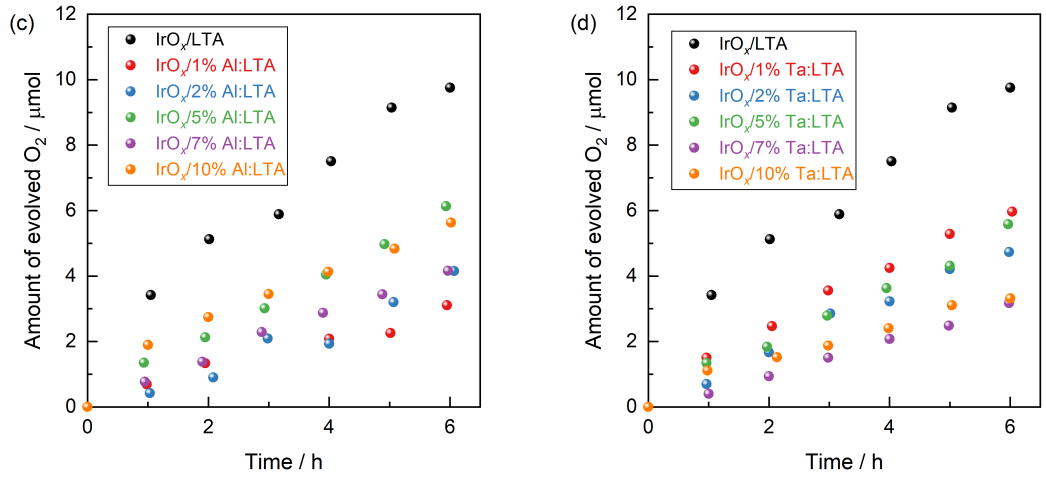

Fig. S8 Time courses of photocatalytic hydrogen evolution half-reactions using (a) Pt/Al:LTA and (b) Pt/Ta:LTA and of photocatalytic oxygen evolution half-reactions using (c) IrO_x/Al:LTA and (d) IrOx/Ta:LTA with different doping levels.

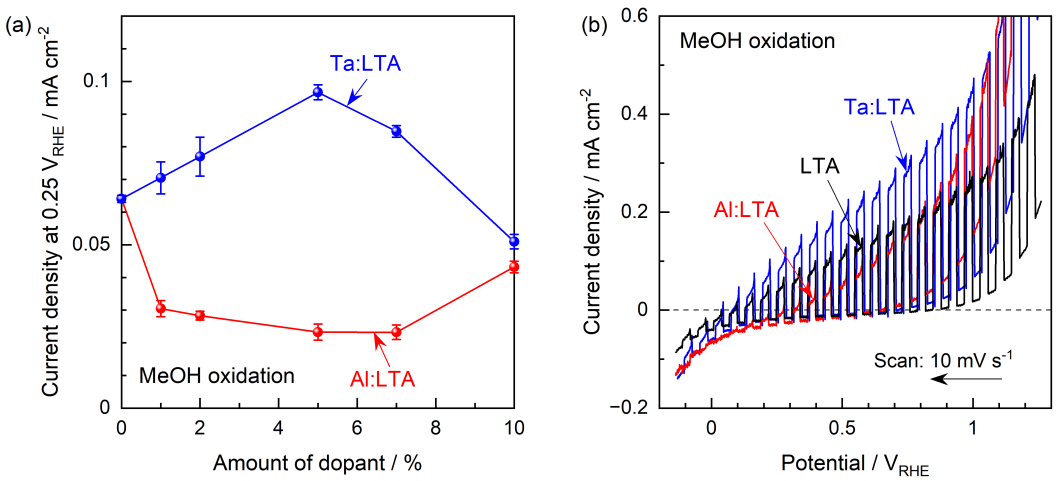

Fig. S9 (a) Current densities for doped LTA photoanodes at an applied potential of 0.25 V_{RHE} under simulated sunlight as functions of the doping level. (b) Typical current-potential curves obtained using LTA, 5%Al-doped LTA and 5%Ta-doped LTA photoanodes without CoPi modification in an aqueous solution containing 0.5 M Na_2SO_4 and 25 vol% methanol.

Half-cell solar-to-hydrogen energy conversion efficiencies

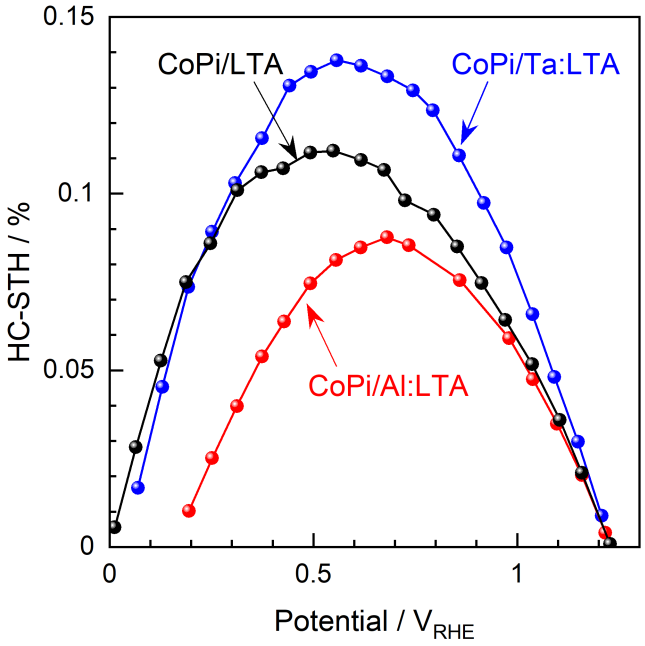

Fig. S10 HC-STH data obtained using CoPi-modified LTA, 5%Al-doped LTA and 5%Ta-doped LTA in aqueous 0.5 M Na_2SO_4 solutions under simulated sunlight.

Effects of Al_2O_3 or Ta_2O_5 impurities

We evaluated the effects of Al_2O_3 or Ta_2O_5 impurities addition on the photocatalytic and PEC performance. The undoped LTA particles were mixed with Al_2O_3 or Ta_2O_5 particles at Al/(Al+Ti) or Ta/(Ta+Ti) molar ratios of 5 mol%, and subsequently calcined at 200 °C for 1 h in air. After modification with 0.5 wt% Pt cocatalysts, photocatalytic activity of the Al_2O_3+LTA specimen during hydrogen evolution half-reaction was assessed. The Ta_2O_3+LTA specimen was fabricated into the shape of photoanode through a PT method and then modified with CoPi cocatalysts for the assessment of PEC oxygen evolution reaction. The results of photocatalysis and PEC reaction using the LTA mixed with Al_2O_3 or Ta_2O_5 impurities were summarized in Fig. S11. Al_2O_3 addition barely changed the photocatalytic hydrogen evolution rate of LTA, while Ta_2O_5 addition slightly decreased the anodic photocurrent especially at the negative potentials. Thus, it can be concluded that the enhancement in photocatalytic and PEC performance discussed in the main manuscript should be attributable to the Al^{3+} or Ta^{5+} doping into the LTA crystalline lattice, and that the excess dopant precursors that were not doped into the photocatalyst crystals barely enhanced the catalytic activity.

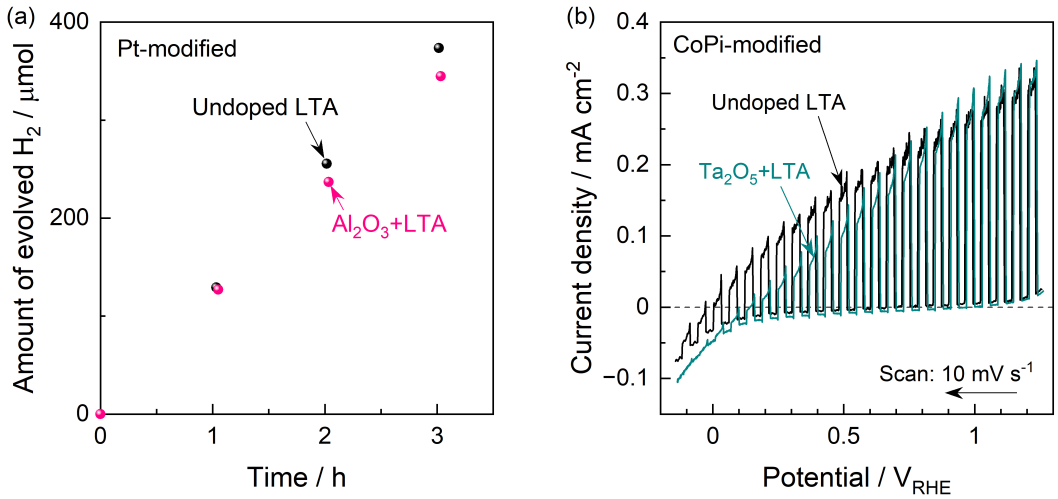

Fig. S11 (a) Time courses of photocatalytic hydrogen evolution half-reactions in an aqueous solution containing 10 mM Na_2S and 10 mM Na_2SO_3 under illumination of 3.00 W Xe lam (λ = 420 - 800 nm) and (b) current-potential curves in aqueous 0.5 M Na_2SO_4 solutions under simulated sunlight using undoped LTA and the specimen mixed with Al_2O_3 or Ta_2O_5.

Preparation of photoanodes for impedance measurements

The backside metal electrode of each particulate photoelectrode prepared by the PT method was partially in contact with the electrolyte through the interstitial spaces between the neighbouring semiconductor particles. This undesired contact was confirmed by electrochemical measurements under dark conditions, as shown in Fig. S12. LTA/Ti fixed on a secondary glass substrate using double-sided carbon tape (i.e., prepared by the standard method) produced a relatively large non-Faradaic current derived from charging of the electric double layer in the Na_2SO_4-based electrolyte. Adding $K_3[Fe(CN)_6]$ to the aqueous electrolyte as a reversible electron acceptor produced a significant cathodic dark current at negative potentials greater than the redox equilibrium potential of $[Fe(CN)_6]^{3-/4-}$. This cathodic current is attributed to the reduction of $[Fe(CN)_6]^{3-}$ at the backside Ti electrode rather than to the reduction reaction driven by the majority carriers (electrons) in the n-type semiconductor. These observations suggest leakage of the conducting metal layer to the electrolyte. If this type of undesirable interface between the metal and electrolyte is present in parallel with the semiconductor/electrolyte interface, the latter circuit may be incorrectly evaluated during the impedance measurements.

In the case that the semiconductor particles/metal foil assembly is fixed by an epoxy resin, the resin penetrates the metal layer and blocks the unwanted exposure of the metal layer.[6] Thus, if the PT photoanode is fabricated using this type of resin, the non-Faradaic current due to charging of the electric double layer in the Na_2SO_4 electrolyte is greatly lowered. A cathodic current resulting from the reduction of $[Fe(CN)_6]^{3-}$ gradually appeared as potentials much more negative than the equilibrium potential were applied. This phenomenon reflects the rectification effect of the semiconductor. That is, electrons in the conduction band of the n-type semiconductor were transferred to the electrolyte only when a sufficiently negative potential was applied, such that the Schottky barrier was no longer present at the semiconductor/electrolyte interface. From these observations, it is apparent that the present LTA photoanodes fixed by an epoxy resin contained solely a semiconductor/electrolyte interface and thus were suitable test samples for the impedance analyses.

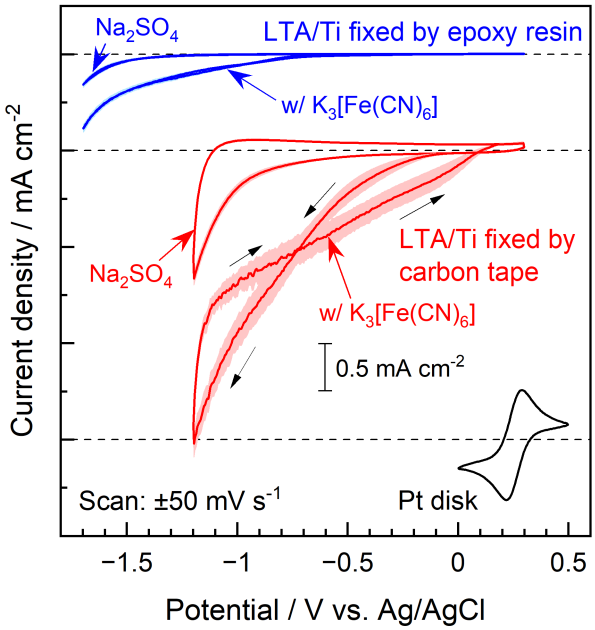

Fig. S12 Current-potential curves for LTA/Ti PT electrodes fixed on secondary glass substrates using double-sided carbon tape or an epoxy resin as acquired under dark conditions in stirred aqueous electrolytes containing 0.5 M Na_2SO_4 with or without 5 mM $K_3[Fe(CN)_6]$. The shaded areas represent the standard error. The cyclic voltammogram obtained for a Pt disk electrode in the same $K_3[Fe(CN)_6]$ solution without forced convection is also included.

Factors limiting the PEC performance of LTA

The effects of modification with CoPi cocatalysts and of the addition of methanol to the electrolyte as a sacrificial reagent are compared in Fig. S13. Neither CoPi modification nor methanol addition appreciably increased the anodic photocurrent generated by the present LTA photoanodes, even though CoPi should accelerate the oxygen evolution reaction kinetics and methanol is oxidized more readily than water. Photocatalysis and PEC reaction rates are typically governed by both physical processes inside the semiconductor and chemical processes at the catalyst surface.[7] Considering that the photocurrent was not increased even in the case that surface chemical reactions proceeded more easily, the photocatalytic and PEC performance of the present LTA specimens appear to have been greatly limited by the sluggish physical processes inside the semiconductor rather than by the rate of surface chemical reactions.

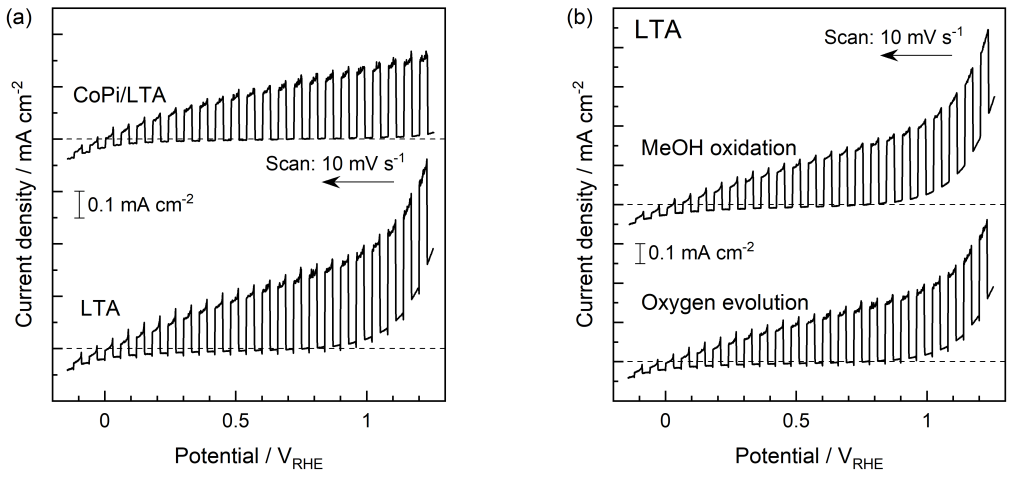

Fig. S13 Comparisons of current-potential curves (a) obtained for LTA photoanodes with and without CoPi cocatalysts in a stirred 0.5 M Na_2SO_4 solution and (b) obtained for bare LTA photoanodes in the same aqueous electrolyte with and without 10 vol% methanol as a sacrificial reagent.

References

1. T. Suzuki, T. Hisatomi, K. Teramura, Y. Shimodaira, H. Kobayashi and K. Domen, *Phys. Chem. Chem. Phys.*, 2012, **14**, 15475
2. T. Minegishi, N. Nishimura, J. Kubota and K. Domen, *Chem. Sci.*, 2013, **4**, 1120.
3. F. Takagi, S. Taguchi, Y. Kageshima, K. Teshima, K. Domen and H. Nishikiori, *Appl. Phys. Lett.*, 2021, **119**, 123902.
4. Y. Wei, G. Cheng, O. Xiong, F. Xu and R. Chen, *ACS Sustainable Chem. Eng.*, 2017, **5**, 5027.
5. K. Maeda, M. Higashi, B. Siritanaratkul, R. Abe and K. Domen, *J. Am. Chem. Soc.*, 2011, **133**, 12334; M. Miyauchi, M. Takashio and H. Tobimatsu, *Langmuir*, 2004, **20**, 232.
6. Y. Kageshima, S. Shiga, H. Kumagai, K. Teshima, K. Domen and H. Nishikiori, *Bull. Chem. Soc. Jpn.*, 2020, **93**, 942.
7. K. Takanabe, *ACS Catal.*, 2017, **7**, 8006.